DC–226 GHz well-impedance-matched high-speed photoreceiver for multi-band signal detection

T. Umezawa[1], P. T. Dat[1], Y. Yoshida[1], S. Nakajima[1], A. Matsumoto[1], K. Akahane[1], A. Kanno[1,2], and N. Yamamoto[1]

1: National Institute of Information and Communications Technology (NICT), 2: Nagoya Institute of Technology
4-2-1, Nukui-Kitamachi, Koganei, Tokyo 184-8795, Japan, toshi_umezawa@nict.go.jp

Abstract: We designed and fabricated a well-impedance-matched ultrabroadband photoreceiver operating beyond 226 GHz and discussed its high data rate multiband performance from the baseband to the W-, D-, and G-bands.

1. Introduction

Multiband communication technology used for multiplexing signals in the frequency domain is one of the attractive options to increase the data rate in both wireless and fiber communication networks. It is well known that dual-band in both the microwave (sub-6: 3.7–4.5 GHz) and millimeter-wave (28 GHz) frequency regions have been used in 5G wireless communication technology [1]. The new radio band, which is the D-band (110–170 GHz), is a promising candidate [2] in beyond 5G (6G) wireless communications along with the conventional microwave and millimeter-wave frequency bands. Discrete multitone (DMT) technology, which multiplexes signals with several multi-bands in a wide frequency range from the DC level to the high-frequency level, has been reported in the high-speed optical fiber communication field. Here, a higher data rate of more than 600 Gbps/λ [3] is achieved by increasing the multitone (band) number in an extended bandwidth and improving the flatness of the frequency response. Therefore, ultra-broadband high-speed photonic devices with a well-impedance-matched design from the baseband (or low-frequency band) to the high-frequency bands (such as the W-, D-, and G-bands) will be the key components in future communication technology (Fig. 1). In this study, we designed and fabricated a well-impedance-matched ultra-broadband photoreceiver within a frequency range of DC–226 GHz and demonstrated high data rate performance in multiple bands from the baseband to the W-, D-, and G-bands.

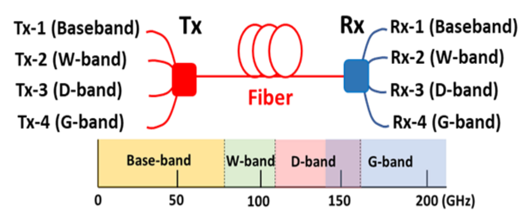

Fig. 1 Concept of multiband communication.

2. DC–226 GHz high-speed photodetector and its characteristics

We designed an ultra-broadband uni-traveling-carrier photodiode (UTC-PD) for a high 3-dB bandwidth over 220 GHz to receive ultra-broadband or multi-band signals within a frequency range of DC–220 GHz. The UTC-PD structure was composed of two main layers (a thin p-doped InGaAs absorption layer and an undoped InP carrier collector layer), which dominated the entire frequency response (see Fig. 2). Here, the carrier concentrations for both the absorption and carrier collection layers were selected in the 10^{18} cm^{-3} range and 10^{14} cm^{-3} range, respectively, and the thickness of each layer was optimized to obtain a bandwidth greater than 200 GHz. A light wave was introduced from the backside of the InP substrate. A high-mesa structure was formed using a dry etching process to define a small photodetection area (p–n junction area) with a diameter of 4–7 µm.

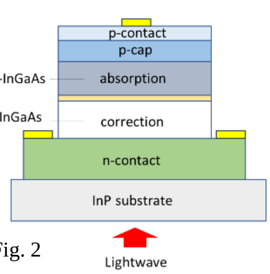

Fig. 2

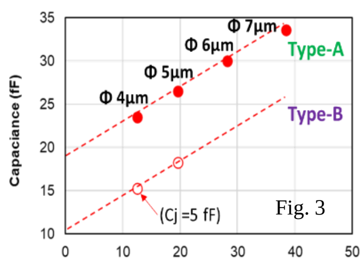

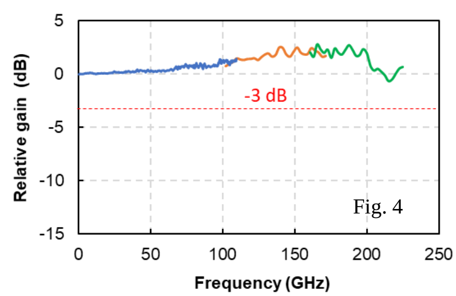

Fig. 2 Cross-sectional view of the UTC-PD design. Fig. 3 Measured capacitance for various junction and electrode sizes (type-A and type-B). Fig. 4 Measured O/E frequency response within a range of DC–226 GHz.

The ground-signal-ground (GSG) electrode design is another key point to achieve a higher bandwidth, in addition to the p–n junction design. By comparing the capacitance values of the two types of electrodes (type-A: 60 × 80 μm, type-B: 50 × 50 μm), we obtained a parasitic capacitance of 18 and 10 fF for the type-A and type-B electrodes, respectively. The parasitic capacitance between the two types of electrodes differs by a factor of approximately 2. The total capacitance of 15 fF can be realized, which comprises the junction capacitance (5 fF) and parasitic capacitance (10 fF), for the 4-μm p–n junction and type-B small electrode design (Fig. 3). To achieve good impedance matching to a 50-Ω load, the distance between the p-n junction location and the 50-Ω matching resistor location should be minimized and optimized. To achieve this, a small-sized 50-Ω matching resistor was fabricated and placed close to the p–n junction. A 110-GHz light wave component analyzer (Keysight: N4372E) was used to measure the frequency response of the baseband signal (10 MHz–110 GHz). An optical heterodyne system with two light wave sources and a power meter (VDI: PM5B) were used for the 110–220 GHz O/E response measurements. A D-band or G-band radio frequency (RF) probe was selected to measure the frequency response in the D-band and G-band, respectively.

As shown in Fig. 4, a very good frequency response was attained within a frequency range of 10 MHz–220 GHz for the three types of measurements. A flat response was observed up to 50 GHz and the response gradually peaked near 180 GHz with a higher gain of 2 dB. The relative gain at 226 GHz was approximately 0 dB against the low-frequency region. A 3 dB bandwidth can be identified at a frequency of over 226 GHz. Figures 5 and 6 show the measured S22 on the Smith chart and the S22 reflectance at 10 MHz–220 GHz, respectively, both of which were measured using a 220-GHz network analyzer (Anritsu: ME7838). Thanks to the design of a 50-Ω matching resistor located near the 4-μm PD, we successfully obtained very good impedance matching to the 50-Ω load in the Smith chart (see Fig. 5), and the S22 reflectance could be preserved below −10 dB from low frequencies up to 140 GHz. Even in the high-frequency region (140–220 GHz), the maximum S22 reflectance was as low as −6 dB (Fig. 6). The responsivity was measured to be 0.1 A/W.

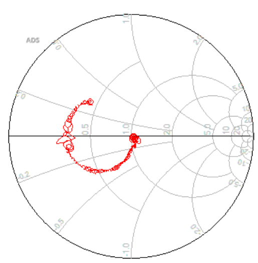
Fig. 5

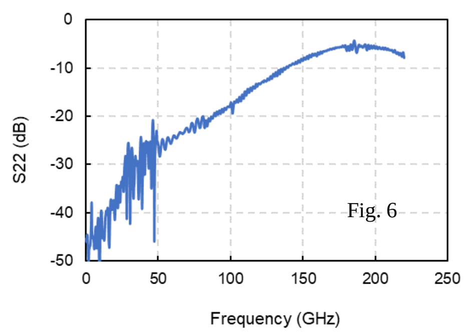

Fig. 6

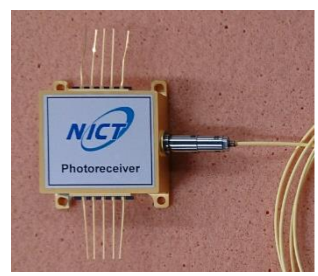

Fig. 7

Fig. 5. Measured S22 on the Smith chart. Fig. 6 S22 output reflectance characteristic within a frequency range of 10 MHz–220 GHz for the fabricated photodetector attached with a 50-Ω matching resistor. Fig. 7 Fabricated PD module.

3. Experimental setup for multiband signal detection

We fabricated a PD module attached to a pigtail fiber (Fig. 7). The butterfly metal package size was 20 × 20 mm, and a 2-μm beam spot was coupled to the 4-μm PD through the optical lens. Because the PD output port was not designed for a multi-parallel output structure for each band, a single output design using a relay transmission substrate connected to the PD output was employed in this experiment. By changing setup-1 to setup-2, both the baseband signal and W-, D-, and G-band signal detection could be achieved. Figure 8 shows the experimental setup for multiband signal detection using the newly developed PD module for high data rate communication. For high

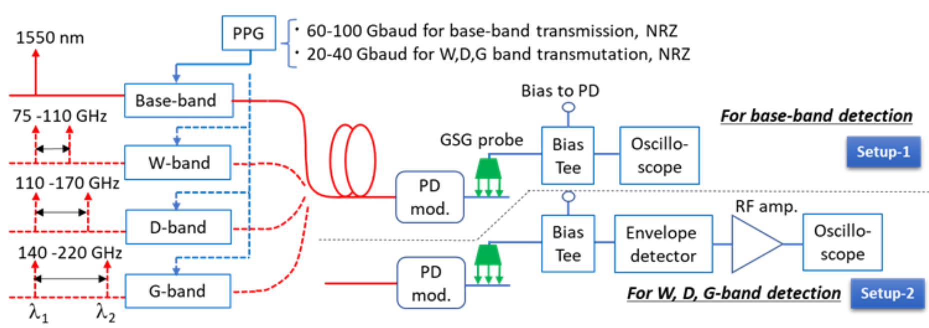

Fig. 8 Experimental setup for multiband detection using the newly developed PD for high data rate communication.

baud rate communication of up to 100 Gbaud in the baseband, a bandwidth of less than 75 GHz is required for the 100-Gbaud signal. The W-band (75–110 GHz) carrier signal, which was located next to the baseband (DC–75 GHz), was generated from an optical two-tone signal with two different wavelengths and was modulated by an intensity modulator in the 20–40 Gbaud range. The 100-Gbaud baseband signal was detected by the PD module using a coaxial RF probe, and the waveform was directly analyzed using an oscilloscope. For the W-, D-, and G-band signal detection, the RF signal through a waveguide-type probe was detected using an envelope detector (Schottky diode) to eliminate the carrier frequency, and the amplified signal without the carrier was analyzed using an oscilloscope.

4. Results and discussion

We demonstrated signal detection with a high baud rate of up to 100 Gbaud (nonreturn-to-zero (NRZ)) in the baseband. By changing the baud rate from 60 to 100 Gbaud, a high-quality eye diagram with a large eye opening was obtained (see the baseband in Fig. 9). Although the bit error rate (BER) was not measured, a very low BER can be expected from the large eye opening in the eye diagrams. On the other hand, the intermediate frequencies (IFs) of 75 and 100 GHz in the W-band were eliminated by using a 15-GHz bandwidth envelope RF detector. Considering the 15-GHz narrow bandwidth of the RF detector, the data rate of the signal was set at 20 Gbaud. Because the G-band (140–220 GHz) overlaps a part of the D-band (110–170 GHz), a G-band RF detector was used for both D- and G-band signal detection. An IF of 162 GHz was selected for D-band signal detection, while an IF of 188–226 GHz was selected for G-band detection. A data rate of 20–40 Gbaud was adopted, considering the 31-GHz bandwidth of the G-band RF detector. In all eye diagrams for the W-, D-, and G-bands, very clear diagrams with large eye openings can be observed (see the W-, D-, and G-bands in Fig. 9). At an IF of 226 GHz, the BER was measured at a data rate of 20 and 40 Gbaud. Very straightforward BER curves were successfully obtained (see Fig. 10), and the BER $< 1\times10^{-6}$ was satisfied for those two data rates. A 1.5-dB power penalty between 20 and 40 Gbaud may be related to the unflatness of the frequency response at 226 GHz or the cut-off frequency of the G-band waveguide.

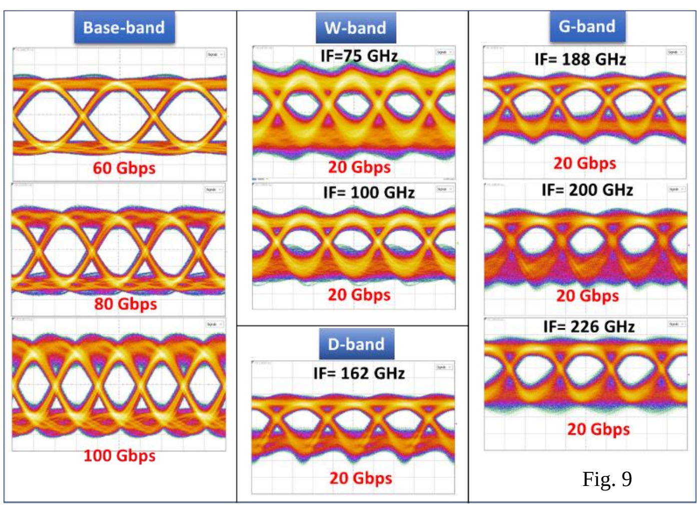

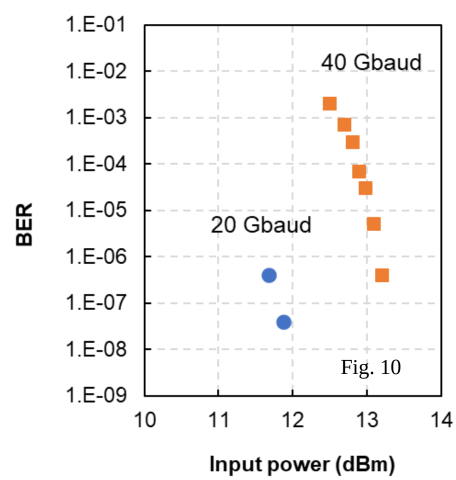

Fig. 9 Eye diagrams at 60–100 Gbaud in the baseband and at 20 Gbaud in the IF = W-, D-, and G-bands. Fig. 10 BER curves at 20 Gbaud (blue) and 40 Gbaud (red), where IF= 226 GHz.

5. Conclusion

We designed and fabricated a well-impedance-matched ultra-broadband photoreceiver, which operated over 226 GHz for the 3-dB bandwidth using the UTC-PD structure. We also optimized the impedance-matching circuit design, and we obtained S22 < −10 dB up to 140 GHz and S22 < −6 dB up to 220 GHz. Based on the discussion on the high data rate multiband performance from the baseband to the W-, D-, and G-bands, we can confirm that there is a high data rate signal detection of 100 Gbaud in the baseband and 20–40 Gbaud in the W-, D-, and G-bands.

This research was conducted in part under the contract “R&D of high-speed THz communication based on radio and optical direct conversion” (JPJ000254) in conjunction with the Ministry of Internal Affairs and Communications of Japan.

6. References

[1] Mario G. L. Frecassetti, et al., Proc. of 16th ISWCS, pp. 427–431, 2019, [2] Norhanis Aida M. Nor, et al., pp. 694-699, ICCCE 2012, 3–5 July 2012, Kuala Lumpur, Malaysia, [3] Xinkuo Yu, et al., W2A. 22 in Proc. of OFC2023